BMC Chemical Engineering

RESEARCH ARTICLE Open Access

Standing-wave Design of Three-Zone, open-loop non-isocratic SMB for purification

David Harvey, Yi Ding and Nien-Hwa Linda Wang*

Abstract

Chromatography with step changes in modulator properties such as pH, solvent strength, or ionic strength to facilitate desorption is widely used in the purification of proteins and other chemicals. Step changes can be incorporated into non-isocratic simulated moving beds; however, applications of such systems have been limited because one must select numerous operating parameters (zone velocities and port velocities). The operating parameters must be selected correctly to achieve high purity, yield, and productivity and depend on a large number of system parameters (feed, material, and equipment parameters). To address this challenge, the Standing-Wave Design method has been developed for three-zone, open-loop, non-isocratic, and non-ideal systems with both linear and non-linear isotherms. This method directly links the operating parameters to the system parameters. The operating parameters can be solved from a set of algebraic equations. In contrast, for non-ideal systems, previous literature design methods require extensive search using rate model simulations, which involve solving partial differential equations at each grid point. Two examples were tested for the effectiveness of the SWD method using rate model simulations. In both examples, sorbent productivity was pressure limited. Higher pressure sorbents or equipment would lead to higher sorbent productivity. In the first example, a 3-zone open-loop simulated moving bed was designed and compared with an optimal batch step-wise elution system. Compared to batch step-wise elution systems, the simulations showed that the 3-zone open-loop SMB could give an order of magnitude higher productivity in systems with weakly competing impurities and two orders of magnitude higher in systems with strongly adsorbing impurities. In the second example, the simulations showed that an SMB designed using the Standing-Wave method could achieve an order of magnitude higher productivity than a system designed using the Triangle Theory.

Background

Stepwise elution is implemented in batch chromatography to reduce cycle time, save solvent, or obtain concentrated products [1–4]. For example, a step change in pH was used in the purification of Immunoglobulin G (IgG), where the protein adsorbed at pH 7.4 and eluted at pH 3 [1]. A step change in solvent strength or ionic strength can also be utilized for biochemical separations [2, 5]. However, if the feed contains strongly competitive impurities, a long column (or a low loading) is needed for the separation of the target product from the impurities, resulting in low column utilization and a diluted product [6]. If the sorbent selectivity is high, column utilization is limited by wave spreading due to mass transfer effects. High column utilization is usually achieved at the cost of a low productivity by using a low flow rate to minimize wave spreading. These limitations of batch chromatography can be mitigated using continuous chromatography as explained below.

If the adsorbent has a perfect selectivity for the target product and all the impurities do not adsorb, one can use a periodic counter current system with three columns for capturing a target product to achieve both high productivity and high column utilization, as shown in Fig. 1 [7, 8]. In the absence of an absorbing impurity, only one column is needed for washing, elution, and regeneration. Moreover, two columns can be used in the loading zone to achieve nearly 100% utilization of the adsorbent capacity if appropriate flow rates are used. The leading column in the loading zone is used for full capacity utilization, and the second column in the loading zone is used to confine the adsorption wave of the target

* Correspondence: wangn@ecn.purdue.edu
Davidson School of Chemical Engineering, Purdue University, West Lafayette, IN, USA

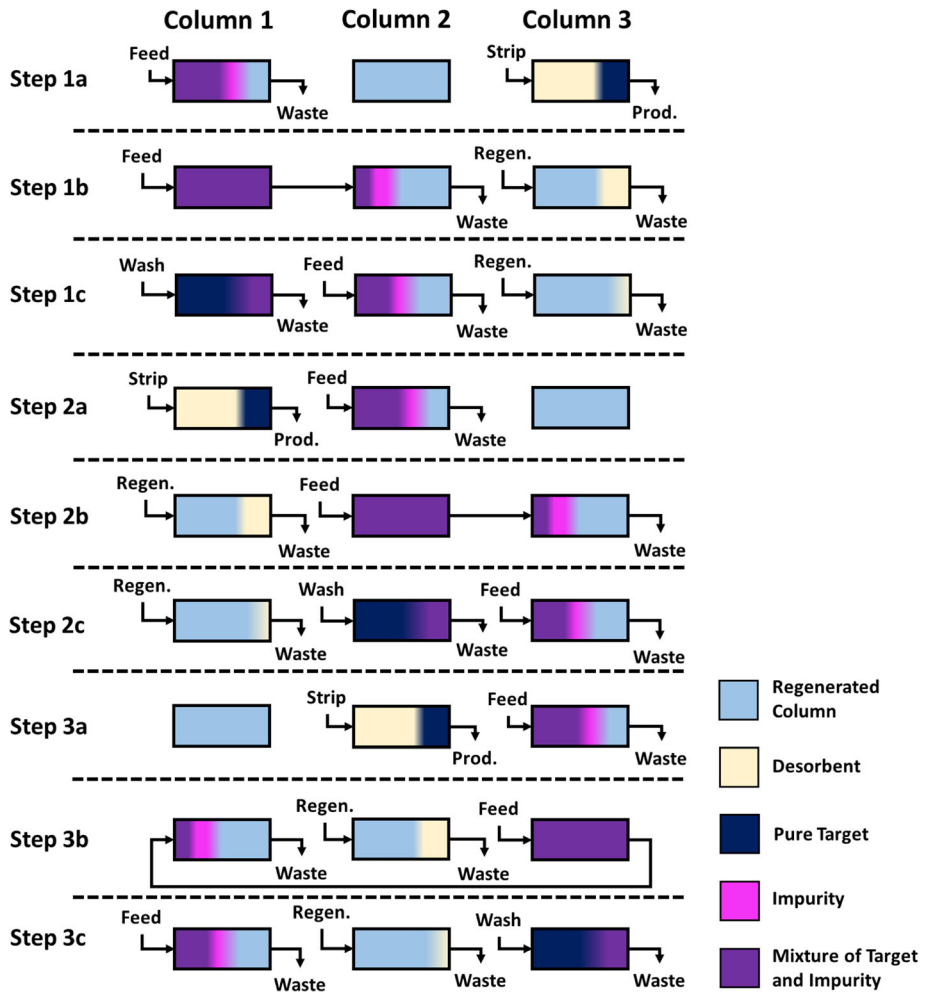

Fig. 1 Example of 3 column periodic counter current separation

product, as shown in Fig. 1. Once the first column is completely loaded, it can be stripped, and the process is repeated using the second and the third column. Periodic counter current systems can also be used in cases without perfect selectivity. However, the yield, purity, or productivity will be reduced compared to systems with perfect selectivity because longer columns, lower flowrates, or reduced purity or yield are required in this case.

Periodic counter current systems are used in a variety of commercial processes; however, they are most useful in biological applications where sorbents are designed to have very high selectivity for the target component [7–10]. The design and optimization of periodic counter current systems is usually done by systematic search using experiments or rate model simulations, which require solving partial differential equations [6, 9, 11–14]. Similar systems with two columns can be used to reduce equipment complexity but sacrifice some column utilization, compared to three column systems [15, 16]. Other techniques such as sequential multi-column chromatography, which adds an additional step to aid in regeneration, and multicolumn countercurrent solvent gradient purification (MCSGP), which is a hybrid of batch and continuous chromatography, can also be used to achieve more efficient separations than batch chromatography [17–19]. By utilizing more effective configurations, sorbent productivity is increased. A detailed discussion of these and other alternative techniques can be found in Steinebach et al. [19].

If the feed contains a competitive impurity, then a periodic counter current system must sacrifice some productivity to produce high-purity product with high yield. For such a system, a 3-zone, non-isocratic, open-loop simulated moving bed can produce a concentrated high-purity product with high yield and high productivity. In a simulated moving bed, products are separated into either a lower affinity raffinate product or a higher affinity extract product. A four-column system is shown in Fig. 2 as an example. Each of the three zones in this configuration has a distinct purpose. The purpose of Zone I is to desorb the target component or the higher

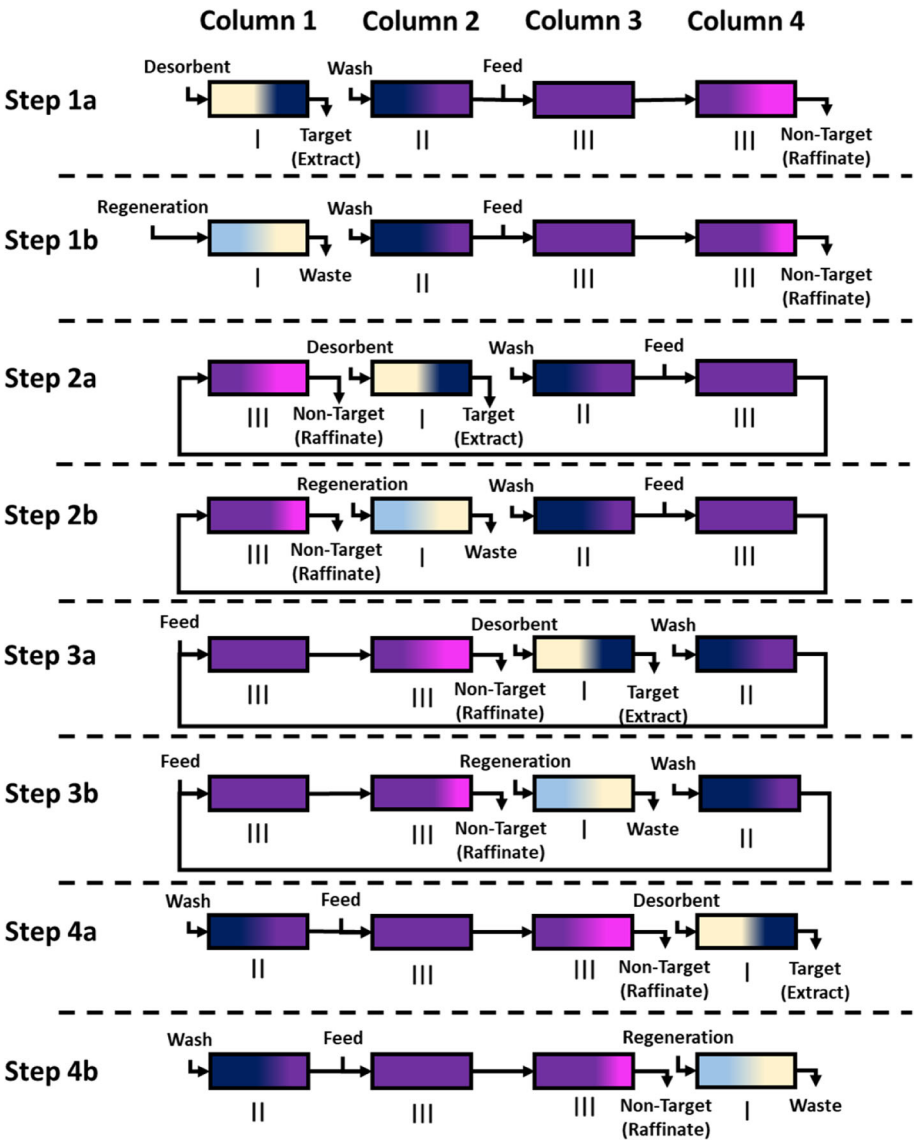

Fig. 2 3-zone open-loop simulated moving bed In Zone III, the feed is loaded into the column. Zone II assures that the less retained component is contained so that it does not leak into the extract product. In Zone I, the desorbent is fed into the column to collect the more retained product as extract. The colors in this figure are the same as Fig. 1

affinity component for collection in the extract product. The affinity of the target component is lower at a lower pH value, for example. In this case, a lower pH solution acts as a desorbent and is fed into Zone I. Because the solvent or the buffer for the target is a non-adsorbing component, the solvent wave or the pH wave will travel quickly through Zone I, allowing for the target component to be desorbed and released into the extract stream. If necessary, Zone I can also be used for regeneration or re-equilibration. Zone II acts as a washing and separation zone. Makeup solvent or buffer at the feed pH is fed into Zone II to elute the remaining weakly adsorbing or non-adsorbing impurity component back into Zone III for collection in the raffinate. Zone II is used to confine the desorption wave of the less adsorbed components and to ensure that they are not collected in the extract product. Zone III is the feed zone. In this zone, the less adsorbed component or any non-adsorbing components are eluted through the column into the raffinate. The adsorption wave of the higher affinity component (in this study, the target) is confined in this zone to prevent its leakage into the raffinate.

A strong desorbent is used in Zone I to facilitate desorption of the target product, resulting in a higher product concentration, shorter processing time, higher solvent efficiency, and higher sorbent productivity. Since

the extract only collects the target product (TP) that is free of the competing impurity (IMP), high product purity can be achieved. High loading is also achieved, because all three zones contain the target and only partial separation of the target band from the impurity bands is needed to recover high-purity product. Furthermore, since elution, separation, and loading occur simultaneously in different zones, overall cycle time is reduced. For these reasons, the 3-zone, open-loop SMB can have much higher product purity, yield, solvent efficiency, and sorbent productivity than conventional batch step-wise elution chromatography. These advantages are especially important for applications involving costly sorbents, high-value products, or fragile products which can degrade during a long processing time. For such applications, it is not important to recycle solvent using a closed-loop system to reduce the overall separation costs.

In previous literature studies, non-isocratic SMB systems have been designed in both closed loop configurations in which a recycle is present and in open-loop configurations without recycle [20–23]. This study will use a 3-zone, open-loop configuration. The open-loop is advantageous because it prevents the mixing of pH, which could also be ionic strength or solvent strength, across different zones. Additionally, recycle is unnecessary in this case because in most protein separations, high product yield is more important than low solvent usage [24]. Without solvent or buffer recycle, a fourth zone is not needed for confining the non-adsorbing or weakly adsorbing components, which can be collected directly in the raffinate. Furthermore, by avoiding mixing the recycle stream with the desorbent stream, the desorbent composition is better-controlled in the open-loop system.

Several challenges exist in the design of 3-zone, non-isocratic non-ideal SMB systems. The well-known Triangle Theory was derived for ideal systems, which have no diffusion or dispersion effects. It can be used to quickly determine the operating parameters for complete separation for ideal systems [25]. However, since the Triangle Theory does not take into account any mass transfer effects in non-ideal systems, the triangle region for ideal systems cannot guarantee purity or yield for non-ideal systems. To ensure product purity and yield for non-ideal systems, grid search using rate model simulations are required within the triangle region [26]. For non-isocratic, non-ideal systems, a new triangle region must be searched for each modulator that is tested, further increasing the number of searches. In contrast, the Standing-Wave Design directly solves the operating conditions that guarantee purity and yield for non-ideal systems. No grid search using rate model simulations is needed. SWD has been proposed for non-isothermal closed-loop systems, but the equations do not apply to non-isocratic open-loop systems [23, 27].

To address these challenges, this study aims to develop a general design method for the 3-zone, open-loop, non-isocratic SMBs for non-ideal systems. Specifically, the objectives are to: (1) develop the Standing-Wave Design (SWD) equations and methods for non-isocratic, 3-zone, open-loop SMB systems with linear or Langmuir isotherms. (2) Verify the SWD using rate model simulations. (3) Compare the effectiveness (productivity, yield, purity, solvent efficiency) of the SWD method with conventional optimal batch stepwise elution systems, and (4) compare the effectiveness of the SWD design method with non-isocratic, non-ideal SMB systems designed based on the Triangle Theory.

The approach taken by this study is as follows. First, the general Standing-Wave Design equations for non-ideal systems are derived for 3-zone, open-loop SMBs. The general equations can be adapted for pH-SMBs with both linear and non-linear isotherms. Solvent strength could be substituted into the general isotherm equations with only minor alterations. Then, the material, feed, and equipment parameters from the literature are used in the new SWD method to obtain a new SMB design. The purity and yield specified in the design method are verified using Aspen Chromatography simulations. The results of the design in terms of productivity, purity, yield and solvent consumption are obtained from the rate model simulations and compared to the experimental literature results.

Some highlights of this study are as follows. The SWD eliminates the need for grid search using rate model simulations, which require solving partial differential equations when designing SMB separations for non-ideal systems. The processing time in the 3-zone SMB is much shorter than for batch step-wise elution, potentially reducing proteolytic degradation of target proteins. Because the SWD requires only solving algebraic equations, it can be used to quickly screen multiple designs or compare different resins to improve the SMB efficiency. Additionally, compared to batch step-wise elution systems, the 3-zone open-loop SMB could give an order of magnitude higher productivity in systems with weakly competing impurities and two orders of magnitude higher productivity in systems with strongly adsorbing impurities.

Methods

The SWD for non-ideal, isocratic, 4-zone SMB systems with linear isotherms was developed by Ma and Wang in 1997 [28]. This method accounted for mass transfer effects and did not require any rate model simulations to determine the operating parameters that can ensure high product purity and high yield. It was paired with optimization techniques to give the overall maximum productivity or minimum cost [29–31]. It was extended

to non-linear isocratic systems [32, 33] and systems with a pressure limit [34–36]. Recently, the SWD equations were solved in terms of dimensionless variables and dimensionless groups for binary and multi-component separations for isocratic systems with linear isotherms [37, 38]. Sorbent productivity and solvent consumption were solved easily for isocratic SMB systems over a wide range of dimensionless operating parameters. The information could be paired with cost functions to find the optimal designs within minutes using a personal computer. The SWD has been extended to systems with different temperatures in different zones, which is the first extension of the SWD to non-isocratic SMBs [23, 27]. These non-isothermal SWD methods only work for temperature swings in 2-zone or 4-zone close-loop SMBs and they do not apply to the 3-zone, open-loop SMBs.

An overview of the input and outputs of both the SWD and rate model simulations utilized in this paper are shown in Fig. 3. The specified yields and system parameters (equipment parameters, material parameters, and feed parameters) are used to solve the SWD equations for the operating parameters, and to predict solvent consumption, product concentrations, and productivity. This can be done without rate model simulations. The operating parameters along with the equipment parameters, material parameters, isotherm parameters, and feed were input into the rate model simulations to verify the yields, solvent consumption, product concentrations, and productivities. A complete notation table is given in Table 1.

Below, the general Standing-Wave equations are derived for non-isocratic, 3-zone, open-loop SMBs. The procedure for solving the equations and other details of the design method are also explained. The isotherms for linear and non-linear non-isocratic systems are introduced first in Section 2.1. The Standing-Wave Design equations for non-isocratic ideal systems are derived in Section 2.2, and the equations for non-ideal systems are derived in Section 2.3. The methodology and the parameters for two examples are given in Section 2.4. A discussion of the rate model simulations can be found in Section 2.5. An overview of the implementation of the SWD method is given in Additional file 1.

Adsorption isotherms

The Standing-Wave Design (SWD) equations are derived first for non-isocratic systems with linear isotherms. In non-isocratic systems, the isotherms are dependent on the composition of the mobile phase. Several factors can affect the adsorption characteristics of a solute, including pH, temperature, solvent strength, or ionic strength. Since the purification of proteins and antibody fragments used as examples were performed using a pH step change, the isotherms will be written as functions of pH. In systems where the solvent strength, ionic strength, or temperature is used to alter adsorption, the isotherms could also be expressed as a function of those variables. A linear isotherm is shown in Eq. (1) where q_i is the solid phase concentration on a solid volume basis of component "i", $a_i(pH)$ is the equilibrium distribution coefficient of component "i" shown as a function of pH, and C_i is the concentration of component "i" in the mobile phase.

$$q_i = a_i(pH)C_i \tag{1}$$

For non-linear systems, which have a concentrated feed with two or more components, the multi-component Langmuir isotherm model can be used to express the competitive adsorption isotherms of multiple solutes. This model is based on competitive, mono-layer adsorption of multiple solutes. Each adsorption site can be considered as located in the center of a square in a lattice, and each solute is smaller than the square. In this model, solute size

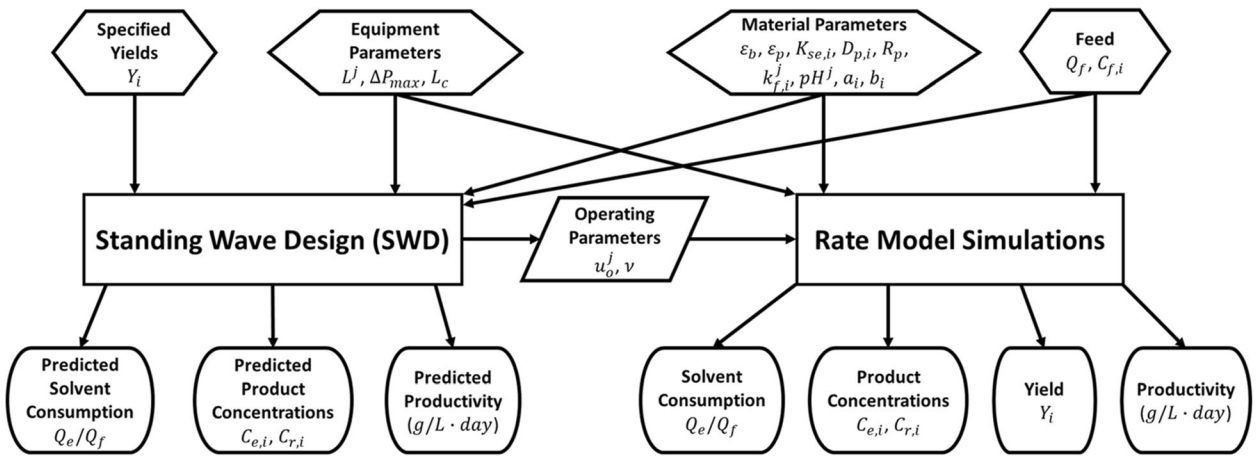

Fig. 3 Overview of Standing Wave Design Inputs and Outputs. Complete list of variable definitions found in Table 1

Table 1 Notation Table of All Variables

Notations	Description	Notations	Description
$a_i(pH)$	Equilibrium distribution coefficient as a function of pH value of component "i" in a linear system, or Langmuir "a" value as a function of pH value of component "i" in a non-linear system.	L_C	Column length
$a_{o,\,i}$, x_i	Adsorption equilibrium constant in Example 2 Eq. (20)	L^j	Length of Zone j
a, b, c	Coefficients in quadratic formula in Eq. (12)	n	pH dependent equilibrium order in Example 1 Eq. (18)
$b_i(pH)$	Langmuir "b" value as a function of pH value in a non-linear system.	P	Phase ratio, $P = \frac{1-\varepsilon_b}{\varepsilon_b}$
C_1^{II}	Concentration of component 1 in the make-up solvent in Zone II	pH^j	pH in Zone j
C_2^{I}	Concentration of component 2 in the desorbent in Zone I	pH_{ref}	Reference pH in Example 1 Eq. (18)
$C_{E,\,i}$	Average concentration of component "i" in the Extract	Q_f	Feed flow rate
$C_{R,\,i}$	Average concentration of component "i" in the Raffinate	Q_j	Flowrate in Zone j
$C_{f,\,i}$	Feed concentration of component "i"	Q_E	Extract flow rate
C_i	Bulk concentration of component "i" in the fluid	Q_R	Raffinate flow rate
$C_{p,\,1}$	Plateau concentration of component 1 (less retained component) in Zone III	q_i	Solid phase concentration on a solid volume basis of component "i"
$C_{p,\,2}$	Plateau concentration of component 2 (more retained component) in Zone II	q_{max}	Sorbent capacity
$C_{s,\,1}$	Plateau concentration of component 1 after feed port in Zone III	R_p	Particle radius
$C^*_{s,1}$	Plateau concentration of component 1 in Zone II before mixing with the feed port	S	Cross-sectional area of the column
$C_{s,\,2}$	Plateau concentration of component 2 after feed port in Zone III	t_s	Step time
$C^*_{s,2}$	Plateau concentration of component 2 in Zone II before mixing with the feed port	u_o^j	Zone velocity
$D_{p,\,i}$	Pore diffusivity of component "i"	$u^j_{w,i}$	Wave velocity of component "i" in Zone j
d_p	Particle diameter	Y_i	Yield of component "i"
$E^j_{b,i}$	Axial dispersion coefficient of component "i" in Zone j	β_i^j	Decay coefficient of component "i" in Zone j.
K_A	Association equilibrium constant in Example 1 Eq. (18)	δ_i^j	Retention factor of component "i" in Zone j
$K_{se,\,i}$	Size exclusion factor of component "i"	ε_b	Bed void fraction
$k^j_{e,i}$	Lumped overall mass transfer coefficient of component "i" in Zone j	ε_p	Particle porosity
$k^j_{f,i}$	Film mass transfer coefficient of component "i" in Zone j	v	Port velocity

or shape does not affect the competitive adsorption [39]. A multi-component Langmuir isotherm is shown in Eq. (2).

$$q_i = \frac{a_i(pH)C_i}{1 + \sum_{j=1}^{n} b_j(pH)C_j} \tag{2}$$

Because the pH, solvent strength, ionic strength, or temperature can affect the affinity for the sorbent and/or the overall capacity, both the "a" and "b" values in Eq. (2) are functions of the modulating variable (in this case pH). It is evident from this equation that the maximum sorbent capacity is equal to a_i/b_i. If a system is run in the isocratic mode, the values of a_i and b_i are held constant. However, the functional form of a_i and b_i can

be changed to fit a variety of modulators or solutes. In this study, two specific functions are used to account for the pH dependence of the isotherms of two different solutes in the two examples in Section 2.4.

Standing-Wave Design for ideal, linear, or non-linear systems

The SWD method for SMB is based on the steady state solution for a true moving bed. For an ideal system, the wave velocity of a key component "i" in zone "j" ($u^j_{w,i}$) is set equal to the average port velocity (ν), which is the column length divided by the step time (Eq. (3d)). If the wave velocity and the port velocity are the same, the wave appears to be "standing" relative to the port and a steady state can be achieved in a true moving bed. The component with the lower sorbent affinity will be labeled component 1 and the component with the higher sorbent affinity is labeled as component 2. For a 3-zone, open-loop binary separation, the wave velocities ($u^j_{w,i}$) of component "i" in zone "j" are matched with the port velocity (ν) shown in Eq. (3).

$$u^I_{w,2} = \nu \tag{3a}$$

$$u^{II}_{w,1} = \nu \tag{3b}$$

$$u^{III}_{w,2} = \nu \tag{3c}$$

$$\nu = \frac{L_c}{t_s} \tag{3d}$$

L_c is the column length, and t_s is the step time. The wave velocity can be expressed in terms of the zone velocity (u^j_o), the phase ratio (P) which is equal to $(1-\varepsilon_b)/\varepsilon_b$ where ε_b is the bed void fraction, and the retention factor (δ^j_i) which is defined in Eqs. (7) and (8).

$$u^j_{w,i} = \frac{u^j_o}{1+P\delta^j_i} \tag{4}$$

Eq. (4) can be rearranged to give the following form:

$$u^I_o = \left(1+P\delta^I_2\right)\nu \tag{5a}$$

$$u^{II}_o = \left(1+P\delta^{II}_1\right)\nu \tag{5b}$$

$$u^{III}_o = \left(1+P\delta^{III}_2\right)\nu \tag{5c}$$

The zone velocities and port velocity can be determined using Eq. (5) paired with the mass balance around the feed port (Eq. (6)). S is defined as the cross-sectional area of the column. Q_f is the feed flow rate.

$$\nu = \frac{Q_f}{S\varepsilon_b P\left(\delta^{III}_2 - \delta^{II}_1\right)} \tag{6}$$

The retention factor for a linear isotherm is shown in Eq. (7).

$$\delta^I_2 = \varepsilon_p + \left(1-\varepsilon_p\right)a^I_2(pH) \tag{7a}$$

$$\delta^{II}_1 = \varepsilon_p + \left(1-\varepsilon_p\right)a^{II}_1(pH) \tag{7b}$$

$$\delta^{III}_2 = \varepsilon_p + \left(1-\varepsilon_p\right)a^{III}_2(pH) \tag{7c}$$

For non-linear, isocratic systems with Langmuir isotherms, the retention factors have been derived previously [23, 27, 34, 35]. The retention factors for non-isocratic, non-linear systems are similar to those for isocratic systems reported previously, except that a_i and b_i are functions of pH or other modulators, as shown in Eq. (8).

$$\delta^I_2 = \varepsilon_p + \left(1-\varepsilon_p\right)a^I_2(pH) \tag{8a}$$

$$\delta^{II}_1 = \varepsilon_p + \frac{\left(1-\varepsilon_p\right)a^{II}_1(pH)}{1+b^{II}_2(pH)C_{p,2}} \tag{8b}$$

$$\delta^{III}_2 = \varepsilon_p + \frac{\left(1-\varepsilon_p\right)a^{III}_2(pH)}{1+b^{III}_1(pH)C_{s,1}+b^{III}_2(pH)C_{s,2}} \tag{8c}$$

Eq. (8) allows for the retention factors to be determined using the plateau concentrations $C_{s,\ i}$ and $C_{p,\ i}$ (see Fig. 4). The plateau concentrations are determined using the Hodograph solutions, shown in Additional File 1 [34]. The subscripts "E" and "R" refer to the average concentration in the extract and raffinate streams, respectively. The superscript Roman numerals refer to the concentration of a component entering that zone. The "*" refers to the concentration before mixing at the feed port.

Standing-Wave Design for non-ideal systems

In non-ideal systems, wave spreading occurs because of mass transfer effects. Wave spreading can cause leakage into the adjacent zones. For this reason, the zone velocities in non-ideal systems must be adjusted to confine the waves in the desired zones. A difference in wave velocity is used to counter wave spreading or "focus" the waves. The wave velocities in the first and second zones must be greater than the port velocity to focus the waves, whereas the wave velocity in the third zone must be smaller than the port velocity to prevent loss of the more retained component (component 2) in the raffinate. The adjusted zone velocities are shown in Eq. (9a-9c), where Δ^j_i is a mass transfer correction term [40]. After substituting in the value of the mass transfer correction term, the adjusted zone velocities are shown in Eq. (9e-g).

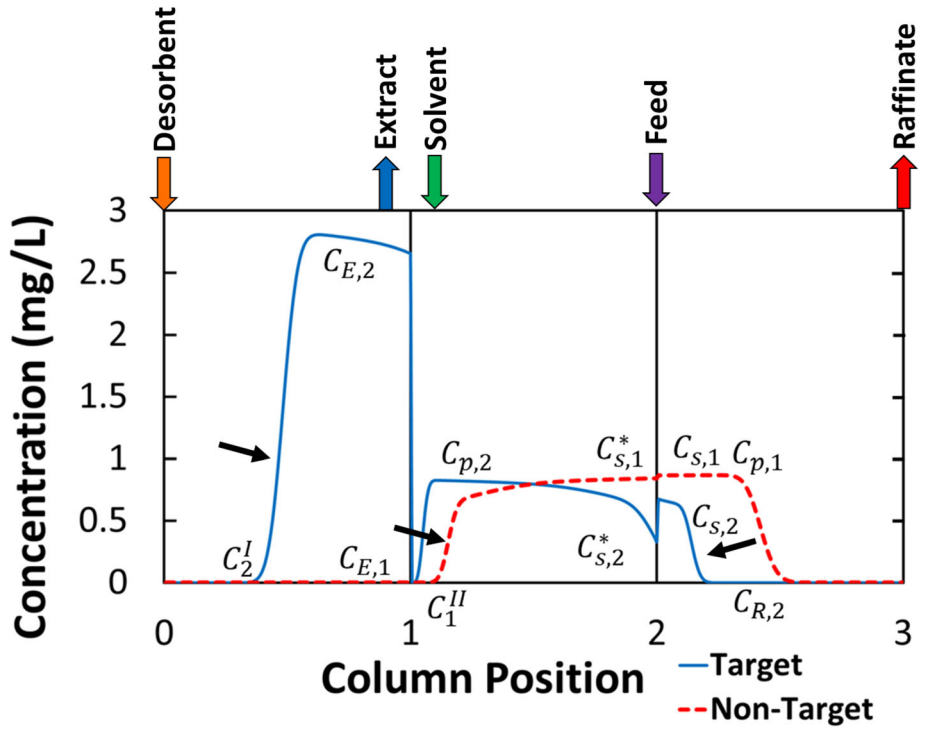

Fig. 4 Example column profile from 3-zone open-loop SMB. The plateau concentrations are denoted with the p and s subscripts. The * denotes the concentration before the feed port. Subscript R and E denotes raffinate concentration and extract concentration respectively. The concentrations with a numeral superscript denote the concentration of the feed into that zone which in both cases listed here is zero. Concentrations shown in middle of step. Profile from Example 1 Case 1

$$u_o^I = \left(1 + P\delta_2^I\right)v + \Delta_2^I \tag{9a}$$

$$u_o^{II} = \left(1 + P\delta_1^{II}\right)v + \Delta_1^{II} \tag{9b}$$

$$u_o^{III} = \left(1 + P\delta_2^{III}\right)v - \Delta_2^{III} \tag{9c}$$

$$\Delta_i^j = \frac{\beta_i^j}{L^j}\left(E_{b,i}^j + \frac{P\delta_i^{j^2}v^2}{k_{e,i}^j}\right) \tag{9d}$$

$$u_o^I = \left(1 + P\delta_2^I\right)v + \frac{\beta_2^I}{L^I}\left(E_{b,2}^I + \frac{P\delta_2^{I\,2}v^2}{k_{e,2}^I}\right) \tag{9e}$$

$$u_o^{II} = \left(1 + P\delta_1^{II}\right)v + \frac{\beta_1^{II}}{L^{II}}\left(E_{b,1}^{II} + \frac{P\delta_1^{II\,2}v^2}{k_{e,1}^{II}}\right) \tag{9f}$$

$$u_o^{III} = \left(1 + P\delta_2^{III}\right)v - \frac{\beta_2^{III}}{L^{III}}\left(E_{b,2}^{III} + \frac{P\delta_2^{III\,2}v^2}{k_{e,2}^{III}}\right) \tag{9g}$$

In Eq. (9), β_i^j is the decay coefficient of component "i" in zone "j", which is defined as the natural log of the ratio of the maximum concentration of component "i" to the minimum concentration of component "i" in zone "j", L^j is the length of zone "j", $E_{b,i}^j$ is the axial dispersion coefficient of component "i" in zone "j", and $k_{e,i}^j$ is the lumped overall mass transfer coefficient of component "i" in zone "j".

$$\frac{1}{k_{e,i}^j} = \frac{R_p^2}{15K_{se,i}\varepsilon_p D_{p,i}} + \frac{R_p}{3k_{f,i}^j} \tag{10}$$

R_p is the particle radius, $K_{se,\,i}$ is the size exclusion factor of component "i", $D_{p,\,i}$ is the intraparticle diffusivity, and $k_{f,i}^j$ is the film mass transfer coefficient of component "i" in zone "j". Eq. (9) can be paired with the mass balance around the feed port (Eq. (11)) to solve for the port velocity.

$$\frac{Q_f}{\varepsilon_b S} = u_o^{III} - u_o^{II} \tag{11}$$

When Eq. (9) is plugged into Eq. (11), the result can be manipulated to give the following quadratic equation form.

$$av^2 + bv + c = 0 \tag{12a}$$

where:

$$a = \frac{\beta_1^{II} P \delta_1^{II\,2}}{k_{e,1}^{II} L^{II}} + \frac{\beta_2^{III} P \delta_2^{III\,2}}{k_{e,2}^{III} L^{III}} \tag{12b}$$

$$b = -P\left(\delta_2^{III} - \delta_1^{II}\right) \tag{12c}$$

$$c = \frac{Q_f}{\varepsilon_b S} + \frac{\beta_1^{II} E_{b,1}^{II}}{L^{II}} + \frac{\beta_2^{III} E_{b,2}^{III}}{L^{III}} \tag{12d}$$

The quadratic formula can then be used to solve for the port velocity which can be used to solve for each of the zone velocities.

The decay coefficients for nonlinear systems are defined below in terms of the maximum and minimum concentrations defined in Fig. 4. The final form is shown on the right in terms of yields, flowrates, known concentrations, and plateau concentrations.

$$\beta_2^I = \ln\left[\frac{C_{E,2}}{C_2^I}\right] = \ln\left[\frac{Y_2}{1-Y_2}\right] \tag{13a}$$

$$\beta_1^{II} = \ln\left[\frac{C_{s,1}^*}{C_1^{II}}\right] = \ln\left[\frac{Q_{II}}{Q_f(1-Y_1)}\right] \tag{13b}$$

$$\beta_2^{III} = \ln\left[\frac{C_{s,2}}{C_{R,2}}\right] = \ln\left[\frac{C_{s,2} Q_{III}}{Q_f C_{f,2}(1-Y_2)}\right] \tag{13c}$$

where $C_{E,\,2}$ is the concentration of component 2 in the extract, $C_{R,\,2}$ is the concentration of the more retained component in the raffinate, C_2^I is the concentration of component 2 that can be leftover in the Zone I while still achieving the target yield. C_1^{II} is the concentration of the less retained component (component 1) that can remain Zone II and still achieve the target yield. $C_{s,1}^*$ is the concentration of component 1 right before the feed port in Zone II, and $C_{s,\,2}$ is the plateau concentration of component 2 after the feed port in Zone III. The values of these terms are adjusted for a 3-zone open-loop system. The β_i^j terms in Eq. (13) can be expressed in terms of zone velocities, known concentrations, and target yields. The concentrations of component 2 in the raffinate and extract are calculated based on the overall mass balance as follows:

$$C_{E,2} = \frac{Q_f Y_2 C_{f,2}}{Q_I} \tag{14}$$

$$C_{R,2} = \frac{Q_f(1-Y_2) C_{f,2}}{Q_{III}} \tag{15}$$

Where Y_2 refers to the yield of component 2 which is specified in the design, $C_{f,\,2}$ is the feed concentration of component 2, Q_f is the feed flow rate, Q_I is the Zone I flow rate or the extract flow rate, and Q_{III} is the Zone III flow rate or the raffinate flow rate. The plateau concentration ($C_{s,\,2}$) is solved using an iterative process as explained in Additional File 1.

C_2^I and C_1^{II} can be determined based on the overall mass balances of component 2 and component 1 respectively. The resulting expressions are shown below.

$$C_2^I = \frac{C_{F,2} Q_F (1-Y_2)}{Q_I} \tag{16}$$

$$C_1^{II} = \frac{C_{F,1} Q_F (1-Y_1)}{Q_{II}} \tag{17}$$

Based on the mass balance at the boundary between Zones II and III, $C_{s,1}^*$ can be approximated using $C_{f,\,1}$. This approximation is based on the assumption that $C_{s,\,1}$ is approximately equal to $C_{R,\,1}$. Substituting Eq. (14–17) into the first from shown in Eq. (13) and making the stated approximations gives the final form of Eq. (13).

The four SWD equations, Eqs. (9), and (12–17), are solved to obtain the four operation parameters (three zone velocities and the port velocity). The value of the decay coefficients and the retention factors are not known when beginning the problem because they are dependent on the plateau concentrations. Therefore, an iterative method must be used to solve for port velocity and zone velocities from the four SWD equations (Eq. (9e-g) and Eq. (11)). An initial guess for the plateau concentrations and decay coefficients is required to solve for the port velocity and zone velocities. Convergence is achieved more quickly if the initial guess is close to the actual solution. For this reason, the solution for ideal systems is obtained first, and used as the initial guess for solving the SWD equations for non-ideal systems.

Example systems

Example 1: Langmuir isotherms with counter-ion modulator

The first example to be discussed in this paper was introduced in Candy et al. 2012. In that study, an IgG sample was separated from a weakly adsorbing impurity using an optimized batch stepwise elution process. The parameters from this example were taken from the literature and they can be estimated using the methods described in Candy et al. [1]. The protein has a high solubility (> 100 g/L) [41]. A silica-based adsorbent, AbSolute, (d_p = 44 μm) was used in a column, 5 mm in diameter and 8.5 cm in length. The optimal loading fraction, length and flowrate were found using a trusted-region simplex search [6]. In the process of Candy et al. 2012, a step change from pH 7.4 to pH 3 was used to elute the target protein. In this study, an open-loop, 3-zone SMB was designed using the same material and feed parameters for comparison with the optimal batch stepwise elution system; however, the pH of the desorbent was 5.4 instead of 3. The feed concentration used was 1 g/L for both the product and the impurity. This was done to assure

that the assumption that the pH wave travels faster than the desorption wave is met. At a pH of 5.4, the target component adsorbs weakly (See Fig. 5). At a pH of 3 or lower, the target eventually becomes approximately non-adsorbing, and thus would move at the same velocity as the pH wave.

The target component isotherm was modeled using a modulated Langmuir isotherm [1]. The modulator in this case is a function of the normalized pH. The Langmuir "a" and "b" values for the target component were:

$$a_i\left(pH^j\right) = q_{max}K_A\left(\frac{pH^j}{pH_{ref}}\right)^n \tag{18a}$$

$$b_i\left(pH^j\right) = K_A\left(\frac{pH^j}{pH_{ref}}\right)^n \tag{18b}$$

In this equation, q_{max} is the sorbent capacity, K_A is the association equilibrium constant, n is the pH dependent equilibrium order, pH_{ref} is a reference pH, and pH^j is the pH in zone "j". The impurity in this example was modeled with a linear isotherm. When this modulated isotherm is matched with a linear isotherm for an impurity, the retention factors are as follows:

$$\delta_2^I = \varepsilon_p + \left(1-\varepsilon_p\right)q_{max}K_2\left(\frac{pH^I}{pH_{ref}}\right)^n \tag{19a}$$

$$\delta_1^{II} = \varepsilon_p + \frac{\left(1-\varepsilon_p\right)a_1^{II}}{1+K_2\left(\frac{pH^{II}}{pH_{ref}}\right)^n C_{p,2}} \tag{19b}$$

$$\delta_2^{III} = \varepsilon_p + \frac{\left(1-\varepsilon_p\right)q_{max}K_A\left(\frac{pH^{III}}{pH_{ref}}\right)^n}{1+K_A\left(\frac{pH^{III}}{pH_{ref}}\right)^n C_{s,2}} \tag{19c}$$

The values of the constants from the literature are given in Table 2 and the effect of pH on the Langmuir "a" value of the target component is shown in Fig. 5. Because the impurity has a linear isotherm that is independent of pH, and the linear "a" value is very low in comparison to the Langmuir "a" value at high pH values, the impurity isotherm is not shown in Fig. 5. The selectivity for this separation is very large (> 100). It is important to note that the Standing-Wave Design equations have been derived on a solid sorbent volume basis. The parameters in the literature and listed later in this paper were on a column volume basis and were converted to a solid volume basis using the bed void fraction and porosity before the SWD equations were solved.

Three columns were used in the design of this SMB because the mass transfer effects were small due to the small size of particles used in this separation. The full simulation parameters for this are given in Table 2. The target yield for this separation was set to 99% for both components.

Because the resin used in this example is a silica-based resin and is thus stable under high pressures (> 690 kPa), a case study was done using this example in which three-zone open-loop pH-SMBs were designed at different pressure limits. The pressures in all cases were calculated using the Ergun equation [42]. In Case 1, the pressure limit used in the study Candy et al. 2012

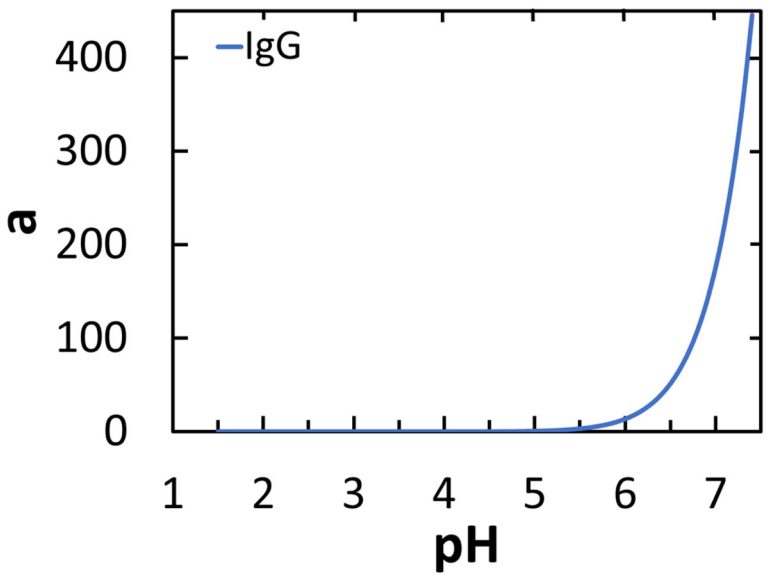

Fig. 5 Langmuir "a" value for target protein for Example 1. The isotherm parameter for the impurity is not shown on this figure because it is a constant 1.6 and would not be easily visible on the scale shown in the figure. Adsorption done at pH 7.4 and desorption done at 5.4

Table 2 Column and Simulation Parameters for Examples 1 and 2

System Parameters								
L_C (cm)	**Number of columns**	**Column Diameter (cm)**	d_p (μm)	ε_b	ε_p	Y	$E^j_{b,i}$	**Film Mass Transfer Coefficient**
2.5	3	Exp. 1: 0.5 Exp. 2: 0.7	Exp. 1: 44 Exp. 2: 34	0.35	0.69	0.99	Chung and Wen	Wilson and Geankoplis
Isotherm Parameters								
Example 1								
Target Compound				**Impurity**				
q_{max}	K_A	pH_{ref}	n	a_1				
73 g/L	6.1 L/g	7.4	16.6	1.6				
Example 2								
$a_{o,\ i}$		x_i		$a_{o,\ i}$			x_i	
0.79		2.01		0.79			2.01	
Simulation Settings and Numerical Parameters								
PDE Discretization Method	**Number of Elements**	**Material Balance Assumption**			**Kinetic Model Assumption**		**Lumped Resistance Film Mode**	
QDS	Exp. 1: 181 Exp. 2: 150	Convection with Estimated Dispersion			Linear Lumped Resistance		Exp. 1: Fluid Exp. 2: Solid	
Mass Transfer/Film Coefficient		**Loading Basis**	**Step Size**				**Integration Method**	
Constant		Volume Basis	0.000005–0.005				Fixed Step Implicit Euler	

(250 kPa) was used for the design. In Case 2, the pressure limit was increased to 690 kPa, which is a common limit for low pressure systems. In Case 3, no pressure limit was set, and the system was limited by the step time. The step time limit was ten seconds. Any value less than ten seconds was considered too short to control accurately. The zone flow rates and step times are given along with the results in Results Section 3.1.

All other parameters not shown in table can be found in Additional file 2. Different Lumped resistance film modes were used based on the available data from the literature sources. Parameters taken from Candy et al. [1] and Cristancho and Seidel-Morgenstern [26].

Example 2: SMB purification of antibody fragments [26]

The second example discussed in this paper is based on a system introduced in Cristancho and Seidel-Morgenstern. In their study, single chain antibody fragments were separated using a simulated moving bed system designed based on the Triangle Theory, without using a search algorithm and rate model simulations to take into account of any mass transfer effects. The material, feed, and equipment parameters were taken from the literature study unless noted otherwise [26]. The columns used in this system were 2.5 cm × 0.7 cm i.d. HisTrap HP columns by GE Healthcare Bio-Sciences. Adsorption and separation occurred at pH 7 whereas desorption occurred at pH 3.8. In this system, both the impurity and the target protein were modeled using a modulated linear isotherm [26]. The form of the isotherms was:

$$q_i = a_{o,i} pH^{x_i} C_i \tag{20}$$

where $a_{o,\ i}$ and x_i are constants. In this example, the impurity competes with the target protein for adsorption. The parameters are listed in Table 2, and the linear isotherm value as a function of pH is shown in Fig. 6. Based on the parameters in Table 2 the selectivity for this system is 3.1 at a pH of 7. The selectivity is reduced to 2.2 at pH 3.8. The selectivity in Example 2 is lower than in Example 1.

For this example, a 3-zone pH SMB was designed with three columns. The small particles in this example also allowed for sharp waves and high product purities with only one column in each zone. The pH-SMB designed using the SWD had the same column length and diameter as the literature example [26]. The target yield of both components was set at 99%. A summary of the simulation and column parameters is given in Table 2, and a summary of the flow rates and step times can be found in Results 3.2. Two case studies were performed in this example to examine the effects of larger particles (80 μm, Case 2) and shorter column length (1 cm, Case 3). The other physical parameters and numerical parameters in all three cases were the same.

Rate model simulations

The simulations of all cases in this study were performed using Aspen Chromatography. The mass balance equation for the Aspen Chromatography model can be found in Additional File 2. The SMB template was modified for the simulations. The isotherms for both examples were

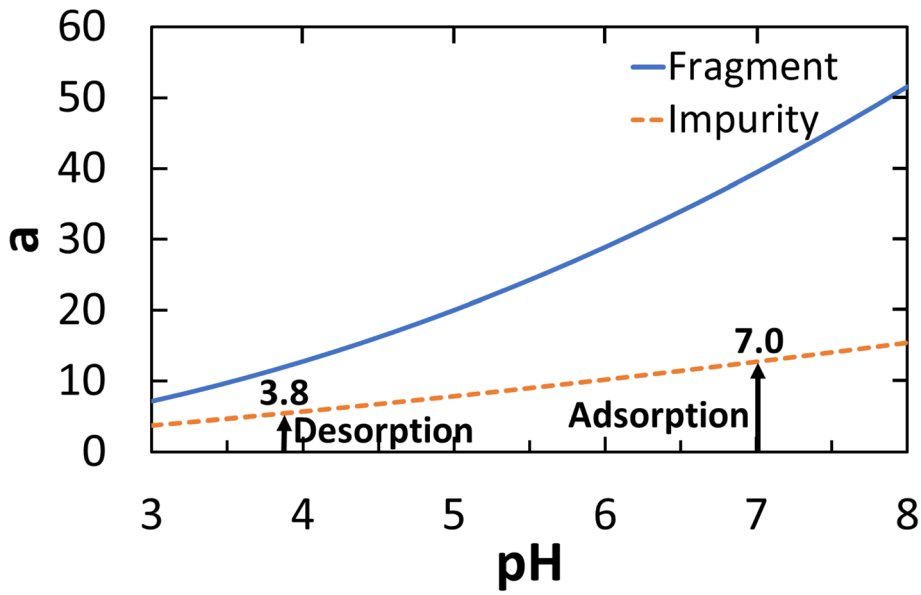

Fig. 6 Isotherm parameters for the fragment and impurity for Example 2. Adsorption will take place at a pH value of 7.0 and desorption will take place at a pH value of 3.8. The selectivity is greater at pH 7.0

programmed into the workbook using the user defined isotherms option. In all simulations, the pH was programmed as an adsorbing component with an equilibrium distribution coefficient of 10^{-5} and thus the pH was approximately non-adsorbing. In each case, the smallest step size in the range given in Table 2 was used to begin each simulation. After the initial step, the step size was increased to the larger value to improve the speed. This was done to prevent instability in Aspen Chromatography during the initial loading of the column. Any parameters that have been changed from the recommended default settings in Aspen Chromatography can be found in Table 2. All other parameters have been left at the default setting for the SMB template.

The SMB simulations in this study did not have dead volume, and the pH was approximated as a non-adsorbing component. Small particles also minimized wave spreading in the column. A combination of these effects allowed for skipping step 1b in Fig. 2. As Column 1 is moved to Zone III in Step 2a, the pH wave moved much faster through the column than the adsorption wave of the target protein. If large dead volume, mass transfer effects, or buffer interactions with the resin could cause the pH wave to spread, there may be a need to allow for equilibration and regeneration between Step 1b and Step 2a. One possible solution to this problem are to add an additional column to Zone III. By adding this additional column, the pH equilibration will happen before the higher affinity product reaches the second column in Zone III. Another possibility is to tune the decay coefficient of Zone I so that it is higher. By raising the velocity in Zone I, this will allow extra time within a step to re-equilibrate the first zone after the extract product is collected. Because dead volume is usually much smaller than column volume in industrial applications, this problem was not considered in this study.

Results

A summary of the results from Example 1 is given in Section 3.1. The results from Example 2 are given in Section 3.2. Because of space limitations, only select profiles are shown in this section; however, an animation showing the column profile development over time for Example 1 Case 1 and Example 2 Case 2 can be found in Additional file 3. The dynamic profiles of all other cases were qualitatively similar to these two example cases.

Results for Example 1

A summary of the results from the three different pressure cases can be found in Table 3. The rate model simulations indicated that the SWD method successfully separated the two components with high-purity (99.9%) and yield (99%). In all three cases, the target yield of 99% was achieved. The product concentration was about 19 g/L in all three cases. The simulated productivity in each case was significantly higher than in batch operation. At the same pressure as the batch operation, the productivity from the SWD pH-SMB was 5 times higher than the batch operation with both a higher yield and a higher product purity (Case 1). The productivity was about 14 times greater than the optimal batch system at the operating limit of low-pressure pumps and columns (Case 2). Solvent

Table 3 Results for Example 1: Comparison with Optimal Batch

Parameter	Separation of Target IgG from a Weakly Adsorbing Impurity			
	Case 1	Case 2	Case 3	Optimal Batch
Column length (cm)	2.5	2.5	2.5	8.5
Pressure limit (kPa)	250	690	2580[a]	250
Number of columns	3	3	3	1
Flow rates (mL/min)	0.78/0.25/15.3 (I/II/III)	2.1/0.68/41.7 (I/II/III)	9.2/2.9/178 (I/II/III)	6.5
Step time (s), pH-SMB	121	44	10	
Cycle time (s)	362	132	30	450
Product conc. (g/L)	19	19	19	4.64
Solvent Consumption (L extract/L feed)	0.05	0.05	0.05	0.4
Purity	99.9	99.9	99.9	98.1
Yield	99.4	99.2	99.4	97.7
Productivity (kg/L/day)	15	40	171	2.9
Normalized Productivity	5.2	13.8	59.0	1

[a]No pressure limit was set in this case. Pressure was calculated using the Ergun Equation [42]

consumption is one-eighth of that of the optimal batch system. Examples of column profiles from Case 1 are shown in Fig. 7. The concentration of the target product is shown in Zone I.

Results for Example 2

The results for three cases for Example 2 are summarized in Table 4. Case 1 used the same particle size (34 μm) and column length (2.5 cm) as the literature case. Case 2 used a larger particle size (80 μm), whereas Case 3 used a shorter column length (1 cm). For all the three cases, the SMBs were designed using the SWD and operated at a maximum pressure of 500 kPa, which is the pressure limit of the resin. The rate model simulations indicated that the SMB designed using the Standing-Wave Design achieved for all three cases the target yield of 99% with a product purity of 99%, which is higher than the best experimental literature case, which gave a purity of 66% and a yield of 91.4%. All three cases had an order of magnitude or higher productivity than the literature case. The productivity in the system with a shorter column length (Case 3) showed higher productivity than both the literature example and the large particle example at the same pressure (Case 2). Examples of the column profile for Case 1 are shown in Fig. 8.

Discussion

A full comparison of a simulated moving bed design using the SWD method with an optimized batch system will be discussed in Section 4.1. Additionally, the implications of the effects of pressure will be discussed as well. In Section 4.2, an SMB designed using SWD will be compared to an SMB designed using the Triangle Theory. The benefits of the Standing-Wave Design method over other design methods will also be discussed.

Discussion of Example 1: comparison with optimal batch stepwise elution

In the example batch system, productivity was optimized by adjusting the step change in pH, column length, loading volume, and elution volumes, while the flowrate was set at the pressure limit (250 kPa). A minimum product purity of 98% was required, meaning that based on the mass balance for a binary mixture of similar concentrations, the target yield was also 98%. In batch stepwise elution separation, a small band overlap was required to achieve 98% purity. Wave spreading due to mass transfer effects limited the productivity of the batch system. To achieve higher than 98% purity, say 99%, in this batch system, the productivity in Table 3 would be reduced as a result of the lower flowrate needed to decrease the wave spreading to meet the purity requirement.

The targeted yield for the SWD was first set at 98% to match the literature study. However, it was found that the optimal flow rate in Zone III for 98% target purity and yield exceeded the pressure limit (250 kPa) and the step-time was lower than 10 s. To operate the Zone III flow rate at the same pressure limit as the batch system, Case 1, the SWD can achieve 99% purity and yield, which are higher than the purity and yield of the batch system, 98%. Rate model simulations were used to verify the SWD of Case 1, and the results listed in Table 3 showed that indeed the target yield of 99% in SWD was achieved.

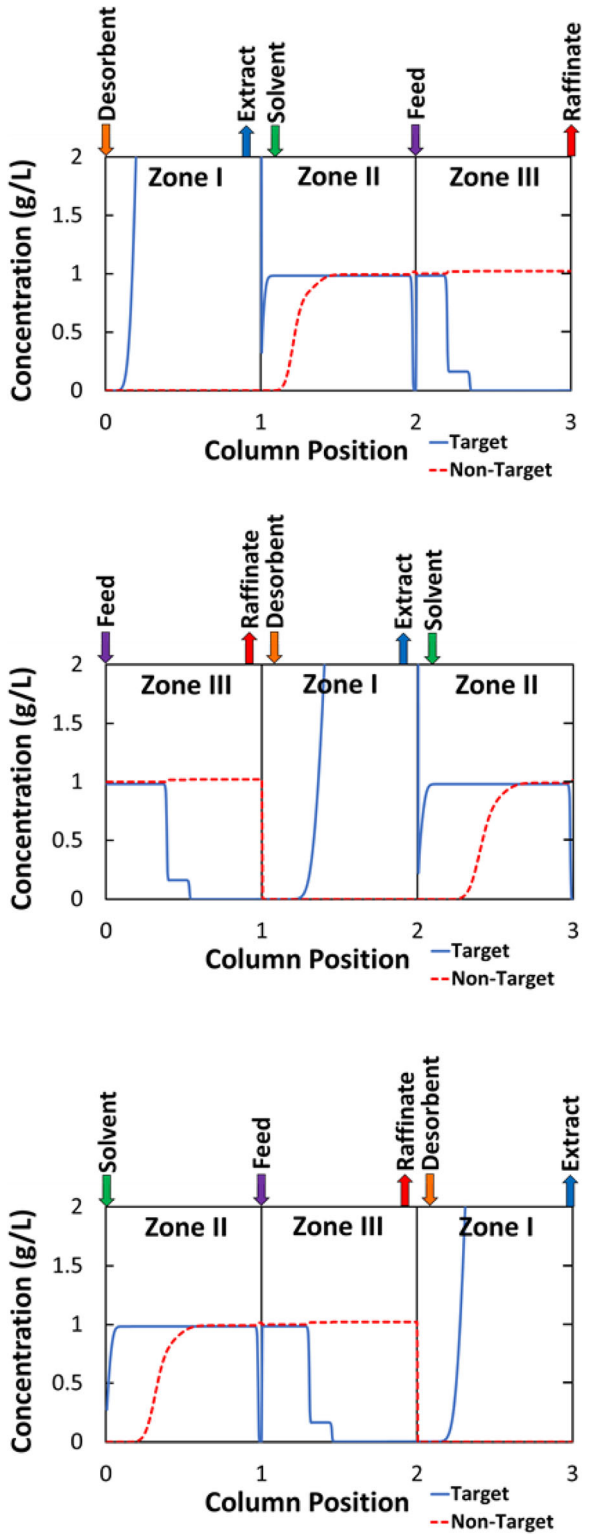

Fig. 7 Example profiles for SMB designed for Case 1 of Example 1 using SWDProfiles shown in the middle of a step.

To further prove that the productivity of Case 1 was limited by the low-pressure requirement (250 kPa), the pressure limit was increased to 690 kPa in Case 2. Again, the rate model simulations of the SWD met the target yield and purity requirement (99%). The productivity was more than doubled compared to Case 1 and an order of magnitude higher than the Optimal Batch case. If the column packed with AbSolute were rated for 690 kPa, then the productivity could be greatly increased without a major increase in the equipment cost.

If high pressure equipment is available (Case 3), the productivity can be further increased for the same purity and yield (99%) with a similar product concentration. In the high-pressure case (Case 3) the pressure was estimated using the Ergun equation to be 2580 kPa. The SWD results showed that the productivity was limited by the step time of 10 s. Still, Case 3 game a productivity about 12 times that of Case 1 and 59 times that of the Optimal Batch case. If the sorbent cost is the major purification cost for this separation, it may be financially beneficial to utilize high pressure equipment for commercial operation.

In all three cases, the rate model simulated yield and purity exceeded the target yield and the target purity in the SWD because the flow rate correction terms in the SWD, Eq. (9) to counter the wave spreading due to mass transfer effects were derived from linear-adsorption isotherm systems. The correction does not account for wave sharpening effects in non-linear isotherm systems. For this reason, the purities and yields achieved in the simulation were even higher than the target values of 99%.

The yield and productivity of SMB in Example 1 are less affected by the mass transfer limitations than those of the batch system because SMB only requires a partial band separation in Zones II and III to achieve high product purity and high yield. This also means that a larger fraction of the bed volume can be used for separation, and the sorbent is used more efficiently. Furthermore, desorption, separation, and loading occur in parallel in SMB; the overall cycle time is reduced compared to batch. If the component is subject to proteolytic degradation, this shorter cycle time can reduce protein degradation during capture and purification. Additionally, a larger fraction of the bed is loaded, leading to a more efficient desorption step because more product can be released. This results in a higher product concentration and a solvent consumption that is potentially 8 times lower than the batch system.

Discussion of Example 2: comparison with literature SMB

The rate model simulations indicated that the simulated moving bed designed using the Standing-Wave Design method could have a productivity that was an order of magnitude higher than one designed using

Table 4 Results for Example 2: Comparison with Literature pH-SMB for the Separation of Target antibody fragments from a competitive adsorbing impurity

Parameter	Case 1	Case 2	Case 3	Literature pH-SMB
Column length (cm)[a]	2.5	2.5	1	2.5
Resin Pressure Limit (kPa)	500	500	500	500
Particle Size (μm)	34	80	34	34
Number of columns	3	3	3	4
Flow rates (mL/min)	12.0/13.1/36.1	86.7/84.1/161.1	27.9/30.8/60.8	1.03/1.02/2.3
	(I/II/III)	(I/II/III)	(I/II/III)	(I/II/III)
Step time (s), pH-SMB	61	10	11	282–324
Cycle time (s)	182	30	33	1128-1269
Product conc. (mg/L)	1.7	0.78	0.95	1.1
Solvent consumption	0.52	1.12	0.93	0.44
(L Extract/L Feed)				
Purity	99	99	99	57–66
Yield	99	99	99	27.4–91.4
Productivity (g/L/day)	10	34	37	0.17–0.58
Normalized Productivity	17–59	58–199	64–220	1

[a]Length of 2.5 cm was selected due to commercial availability of this column size. The inner diameter of the columns in both cases was 0.7 cm

the Triangle Theory. It was noted in Cristancho and Seidel-Morgenstern that their pH-SMB was not optimized. To determine the best zone flow rates to achieve desired product purity and yield in non-ideal systems, the Triangle Theory involves a systematic search using rate-model simulations which require solving partial differential equations. The Standing-Wave Design method allows for a high productivity, high-purity, and high yield design without search using rate model simulations. While the results were verified using rate model simulations, the design solution was obtained in less than a second because the four Standing-Wave Design equations are algebraic equations, not partial differential equations.

The SMB system in the literature had a wide pH front, which may have, along with the design method which was not optimized, contributed to the low purity and yield in the literature system. The dead volume in columns for commercial production should be reduced, causing the pH waves to sharpen and improving the product purity and yield.

It is also important to note that the pressure limited the productivity of this system. The sorbent pressure limit was 500 kPa. A more robust sorbent with similar adsorption properties would increase the sorbent productivity. If the pressure limits the zone flow rates, one cannot operate at the maximum flow rate allowable by the mass transfer parameters. This is evident in Example 2, Case 2. The system with 80-μm particles (Case 2) had an increased overall productivity because larger particles allowed for faster flow at the same column length. Because Case 1 was not limited by the mass transfer effects, larger particles could be used in Case 2 without a reduction in purity. For the same column length, larger particles can be used to increase the productivity for this system. Alternatively, a shorter column with 34 μm particles (Case 3) would allow a higher feed flowrate to increase the productivity. Larger particles or shorter columns may help increase the productivity in Example 1 as well because the productivity is similarly limited by the pressure and not by the mass transfer efficiency.

Example 2 also indicates that the SMB gives even higher advantages over batch systems when there is a competitive impurity. The rate model simulations of the SMB designed using the SWD gave productivities that were an order of magnitude better than the SMB designed using the Triangle Theory, which was already an order of magnitude more productive than a batch system for the same separation [26]. That means that it is possible for an SMB designed using SWD is two orders of magnitude more productive than the reported optimal batch systems. The benefits compared to batch systems are greater for Example 2, because the feed contains a more competitive impurity. While the rate model simulations indicate that a two order of magnitude increase is possible in batch systems with a competitive impurity, experimental verification is needed in future studies.

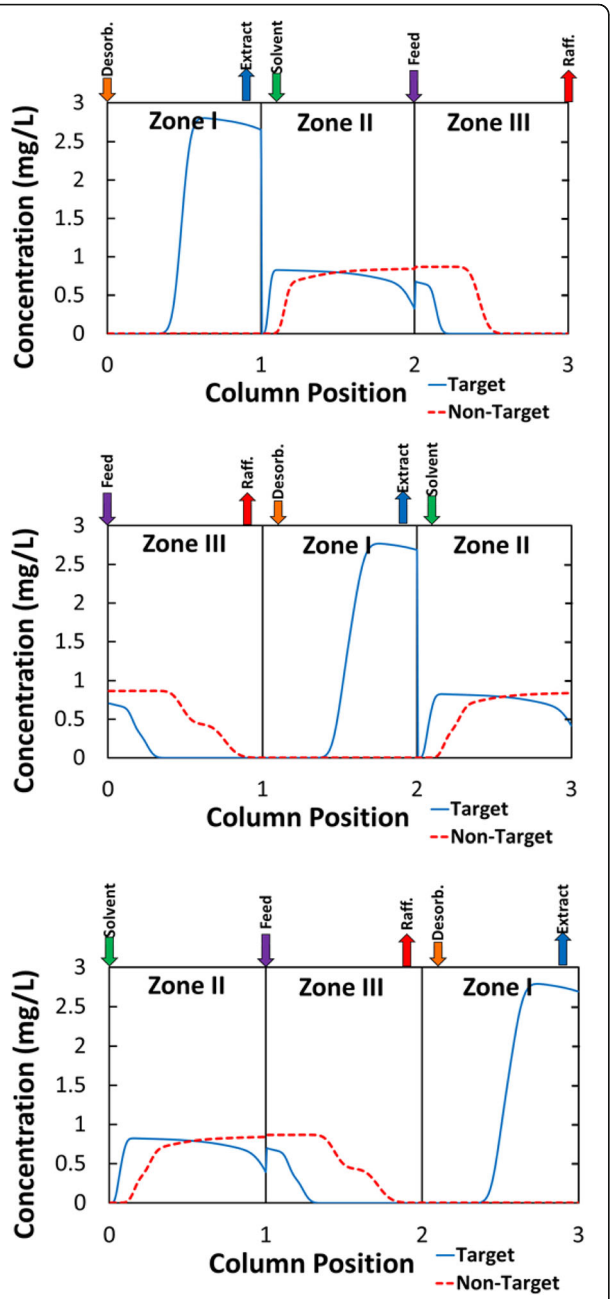

Fig. 8 Example profiles for SMB designed for Case 1 of Example 2 using SWD. Profiles shown at the middle of a step

Conclusions

Although the pH-SMB has shown potential for higher sorbent productivities and higher purity and yield separations than batch chromatography for non-isocratic systems, the use of pH-SMB systems has been limited. One reason for this limited use is the increased complexity compared to batch systems. The large number of system parameters make the design of effective non-isocratic SMBs challenging. To overcome this barrier, we developed a new design method that can find the operating parameters to achieve high product purity and high yield. The design method was verified using rate model simulations.

This study documents the theoretical foundation, equations, and algorithm of the Standing-Wave Design method for non-isocratic systems. The general equations for the Standing-Wave Design of non-isocratic and non-ideal systems were developed for both linear and non-linear isotherms. The Standing-Wave Design method allows for fast and efficient design of SMB systems without extensive search in the four-parameter space. In Example 1, rate model simulations indicated that the 3-zone, open-loop SMB achieved higher purity and yields and potential productivities between 5 and 14 times higher than that of an optimal batch step-wise elution system with low pressure equipment. In Example 2, the SMB system designed using the new SWD method showed an order of magnitude higher potential productivity compared to the pH-SMB designed using the Triangle Theory method. The SMB designed using the SWD method also produced products with higher purity and higher yield. In both examples, the pressure drop was the limiting factor for the feed flow rate in the system. Therefore, using larger particles or shorter columns could achieve a higher productivity because they allowed for higher flow rates. Higher pressure columns and equipment allow for higher productivity. Furthermore, the advantages of a 3-zone, non-isocratic SMB are most significant if the feed has a strongly competitive impurity. The ability to design efficient systems quickly without any trial-and-error experiments or simulations helps remove a major barrier for the application of the three-zone, open-loop SMB. Compared to batch step-wise elution systems, the 3-zone, open-loop SMB could potentially give an order of magnitude higher productivity in systems with weakly competing impurities and two orders of magnitude higher productivity in systems with strongly adsorbing impurities.

Additional files

Additional file 1: Implementation of the Standing-Wave Design for Non-Isocratic Systems. This additional file gives a more in depth look at the application of the SWD and gives general algorithms to implement the design method in new systems. (PDF 757 kb)

Additional file 2: Aspen Chromatography Model. This file gives the mass balance equation that was utilized in Aspen chromatography for the rate model simulations performed in this study as well as the operating parameters not given in the complete body of the text. (PDF 101 kb)

Additional File 3: Animation of Profile Developments. This data is an animated profile of the columns from Example 1 Case 1 and Example 2 Case 1 from the manuscript. It shows the concentration of each component in the column at different times throughout the cycle. (PPTX 9040 kb)

Abbreviations
IgG: Immunoglobulin G; SMB: Simulated Moving Bed; SWD: Standing-Wave Design

Acknowledgements
We would like to acknowledge the contributions of Nicholas Soepriatna for his preliminary work.

Endnotes
'Not applicable'

Funding
This study was supported by the National Science Foundation (CBET 1403854), Purdue Process Safety and Assurance Center, and the Davidson School of Chemical Engineering, Purdue University.

Availability of data and materials
Data are available within the text of the paper and within Additional files 2 and 3.

Authors' contributions
Mr. DH. derived the model equations, developed the simulations, and contributed to writing the manuscript. Prof. LW conceived the project and contributed to the derivation of the model equations, evaluation of the results, and writing the manuscript. Mr. YD contributed to the simulations and writing the manuscript. All authors have read and approve of the final manuscript.

Competing interests
The authors declare that they have no competing interests.

Publisher's Note

Received: 22 January 2019 Accepted: 14 May 2019
Published online: 25 July 2019

References
1. Ng CKS, Osuna-Sanchez H, Valéry E, Sørensen E, Bracewell DG. Design of high productivity antibody capture by protein a chromatography using an integrated experimental and modeling approach. J Chromatogr B. 2012;899:116–26. https://doi.org/10.1016/j.jchromb.2012.05.010.
2. Ma Z, Tanzil D, Au BW, Wang NHL. Estimation of solvent-modulated linear adsorption parameters of taxanes from dilute plant tissue culture broth. Biotechnol Prog. 1996;12:810–21.
3. Yamamoto S, Kita A. Rational design calculation method for stepwise elution chromatography of proteins. Food Bioprod Process. 2006;84(1 C):72–7.
4. Hjerten S, Levin O, Tiselius A. Protein chromatography on calcium phosphate columns. Arch Biochem Biophys. 1956;65:132.
5. Yamamoto S, Suehisa T, Sano Y. Preparative separation of proteins by gradient- and stepwise-elution chromatography: Zone-sharpening effect. Chem Eng Commun. 1993;119:221–30.
6. Ng CKS, Rousset F, Valery E, Bracewell DG, Sorensen E. Design of high productivity sequential multi-column chromatography for antibody capture. Food Bioprod Process. 2014;92:233–41. https://doi.org/10.1016/j.fbp.2013.10.003.
7. Warikoo V, Godawat R, Brower K, Jain S, Cummings D, Simons E, et al. Integrated continuous production of recombinant therapeutic proteins. Biotechnol Bioeng. 2012;109:3018–29.
8. Mahajan E, George A, Wolk B. Improving affinity chromatography resin efficiency using semi-continuous chromatography. J Chromatogr A. 2012;1227:154–62. https://doi.org/10.1016/j.chroma.2011.12.106.
9. Pollock J, Bolton G, Coffman J, Ho SV, Bracewell DG, Farid SS. Optimising the design and operation of semi-continuous affinity chromatography for clinical and commercial manufacture. J Chromatogr A. 2013;1284:17–27.
10. Godawat R, Konstantinov K, Rohani M, Warikoo V. End-to-end integrated fully continuous production of recombinant monoclonal antibodies. J Biotechnol. 2015;213:13–9. https://doi.org/10.1016/j.jbiotec.2015.06.393.
11. El-Sabbahy H, Ward D, Ogonah O, Deakin L, Jellum GM, Bracewell DG. The effect of feed quality due to clarification strategy on the design and performance of protein A periodic counter-current chromatography. Biotechnol Prog. 2018;34:1380–92. https://doi.org/10.1002/btpr.2709.
12. Carta G, Perez-Almodovar EX. Productivity considerations and design charts for biomolecule capture with periodic countercurrent adsorption systems. Sep Sci Technol. 2010;45:149–54.
13. Ernest MV, Bibler JP, Whitley RD, Wang NHL. Development of a carousel ion-exchange process for removal of Cesium-137 from alkaline nuclear waste. Ind Eng Chem Res. 1997;36:2775–88. https://doi.org/10.1021/ie960729+.
14. Liapis AI, Rippin DWT. The simulation of binary adsorption in continuous countercurrent operation and a comparison with other operating modes. AICHE J. 1979;25:455–60.
15. Angarita M, Müller-Späth T, Baur D, Lievrouw R, Lissens G, Morbidelli M. Twin-column CaptureSMB: a novel cyclic process for protein A affinity chromatography. J Chromatogr A. 2015;1389:85–95. https://doi.org/10.1016/j.chroma.2015.02.046.
16. Baur D, Angarita M, Müller-Späth T, Morbidelli M. Optimal model-based design of the twin-column CaptureSMB process improves capacity utilization and productivity in protein A affinity capture. Biotechnol J. 2016;11:135–45. https://doi.org/10.1002/biot.201500223.
17. Aumann L, Morbidelli M. A continuous multicolumn countercurrent solvent purification (MCSGP) process. Biotechnol Bioeng. 2007;988:1043–55.
18. Müller-Späth T, Aumann L, Melter L, Ströhlein G, Morbidelli M. Chromatographic separation of three monoclonal antibody variants using multicolumn countercurrent solvent gradient purification (MCSGP). Biotechnol Bioeng. 2008;100:1166–77. https://doi.org/10.1002/bit.21843.
19. Steinebach F, Müller-Späth T, Morbidelli M. Continuous counter-current chromatography for capture and polishing steps in biopharmaceutical production. Biotechnol J. 2016;11:1126–41.
20. Abel S, Mazzotti M, Morbidelli M. Solvent gradient operation of simulated moving beds. J Chromatogr A. 2004;1026:47–55. https://doi.org/10.1016/j.chroma.2003.11.054.
21. Abel S, Mazzotti M, Morbidelli M. Solvent gradient operation of simulated moving beds - 2. Langmuir isotherms. J Chromatogr A. 2004;1026:47–55.
22. Migliorini C, Wendlinger M, Mazzotti M, Morbidelli M. Temperature gradient operation of a simulated moving bed unit. Ind Eng Chem Res. 2001;40:2606–17.
23. Soepriatna N, Wang NHL, Wankat PC. Standing Wave Design and Optimization of Nonlinear Four-Zone Thermal Simulated Moving Bed Systems. Ind Eng Chem Res. 2015;54:10419–33.
24. Kelly B. Industrialization of MAb production technology. MAbs. 2009:443–52. https://doi.org/10.4161/mabs.1.5.9448.
25. Mazzotti M, Storti G, Morbidelli M. Optimal operation of simulated moving bed units for nonlinear chromatographic separations. J Chromatogr A. 1997;769:3–24. https://doi.org/10.1016/S0021-9673(97)00048-4.
26. Martínez Cristancho CA, Seidel-Morgenstern A. Purification of single-chain antibody fragments exploiting pH-gradients in simulated moving bed chromatography. J Chromatogr A. 2016;1434:29–38. https://doi.org/10.1016/j.chroma.2016.01.001.
27. Soepriatna N, Wang NHL, Wankat PC. Standing Wave Design of 2-Zone Thermal Simulated Moving Bed Concentrator (TSMBC). Ind Eng Chem Res. 2015;54:12646–63.
28. Ma Z, Wang N-HL. Standing Wave Analysis of SMB Chromatography: Linear Systems. AICHE J. 1997;43:2488–508.
29. Lee KB, Kasat RB, Cox GB, N-HL W. Simulated moving bed multiobjective optimization using standing wave design and genetic algorithm. AICHE J. 2008;54:2852–71.
30. Cauley FG, Cauley SF, Lee KB, Xie Y, Wang NHL. Standing wave annealing technique: For the design and optimization of nonlinear simulated moving bed systems with significant mass-transfer effects. Ind Eng Chem Res. 2006;45:8697–712.
31. Cauley FG, Xie Y, N-HL W. Optimization of SMB systems with linear adsorption isotherms by the standing wave annealing technique. Ind Eng Chem Res. 2004;43:7588–99. https://doi.org/10.1021/ie049842n.
32. Lee KB, Mun S, Cauley F, Cox GB, Wang NHL. Optimal Standing-Wave Design of Nonlinear Simulated Moving Bed Systems for Enantioseparation. Ind Eng Chem Res. 2006;45:739–52.
33. Xie Y, Farrenburg CA, Chin CY, Mun S, Wang NHL. Design of SMB for a nonlinear amino acid system with mass-transfer effects. AICHE J. 2003;49:2850–63.
34. Lee KB, Chin CY, Xie Y, Cox GB, Wang NHL. Standing-Wave Design of a Simulated Moving Bed under a Pressure Limit for Enantioseparation of Phenylpropanolamine. Ind Eng Chem Res. 2005;44:3249–67.

35. Mallmann T, Burris BD, Ma Z, Wang NHL. Standing Wave Design of Nonlinear SMB Systems for Fructose Purification. AIChE J. 1998;44:2628–46.
36. Lee HJ, Xie Y, Koo YM, Wang NHL. Separation of lactic acid from acetic acid using a four-zone SMB. Biotechnol Prog. 2004;20:179–92.
37. Weeden GS, Wang NL. Speedy standing wave design, optimization, and scaling rules of simulated moving bed systems with linear isotherms. J Chromatogr A. 2017;1493:19–40. https://doi.org/10.1016/j.chroma.2017.02.038.
38. Harvey D, Weeden G, Wang NHL. Speedy standing wave design and simulated moving bed splitting strategies for the separation of ternary mixtures with linear isotherms. J Chromatogr A. 2017;1530:152–70. https://doi.org/10.1016/j.chroma.2017.10.050.
39. Langmuir I. THE ADSORPTION OF GASES ON PLANE SURFACES OF GLASS, MICA AND PLATINUM. J Am Chem Soc. 1918;40:1361–403. https://doi.org/10.1021/ja02242a004.
40. Hritzko BJ, Xie Y, Wooley RJ, N-HL W. Standing-wave design of tandem SMB for linear multicomponent systems. AIChE J. 2002;48:2769–87. https://doi.org/10.1002/aic.690481207.
41. Wang Y, Lomakin A, Latypov RF, Laubach JP, Hideshima T, Richardson PG, et al. Phase transitions in human IgG solutions. J Chem Phys. 2013;139:1–9.
42. Ergun S. Fluid Flow through Packed Columns. J Chem Eng Prog. 1952;48:89–94.